

Nematic-Like Alignment in SWNT Thin Films from Aqueous Colloidal Suspensions

Budhadipta Dan,^{†,‡} Anson W. K. Ma,^{‡,§,||} Erik H. Háróz,^{‡,⊥} Junichiro Kono,^{†,‡,⊥} and Matteo Pasquali^{*,‡,§,#}

[†]Department of Physics and Astronomy, [‡]Department of Chemical and Biomolecular Engineering, [⊥]Department of Electrical and Computer Engineering, [#]Department of Chemistry, and [§]R.E. Smalley Institute for Nanoscale Science & Technology, Rice University, 6100 Main Street, Houston, Texas 77005, United States

Supporting Information

ABSTRACT: We present a modification of the vacuum filtration technique for fabricating transparent conductive SWNT thin films with local nematic-like orientational ordering. Dilute SWNT surfactant dispersions are filtered through a vacuum filtration setup in a slow and controlled fashion. The slow filtration creates a region of high SWNT concentration close to the filter membrane. While slowly moving through this region, SWNTs interact and align with each other, resulting in the formation of thin films with local nematic ordering. Scanning electron microscopy and image analysis revealed a local scalar order parameter (S_{2D}) of 0.7–0.8 for slow filtration, three times higher than those produced from “fast filtration” ($S_{2D} \approx 0.24$). Orientational ordering is demonstrated with different stabilizing surfactants, as well as with dispersions enriched in metallic SWNTs, produced by density-gradient ultracentrifugation. Simple estimates of relative convective versus diffusive transport highlight the main differences between slow versus fast filtration and the resulting SWNT concentration profiles. Comparisons with previous studies on three stages of liquid-crystal phase transition provide insight into the spontaneous ordering process, indicating the lack of a “healing stage”, which results in a microstructure consisting of staggered domains in our SWNT films.

INTRODUCTION

Despite nearly two decades of intense research, translation of the extraordinary properties of individual carbon nanotubes (CNTs)^{1,2} into macrostructures^{3,4} still remains challenging. Specifically, electrical properties are limited by junction resistance, due to a combination of CNT misalignment and mismatch in electronic band structure in the case of single-walled carbon nanotubes (SWNTs) of different chirality.⁵ Likewise, mechanical properties are limited by incomplete alignment and poor packing due to polydisperse CNT diameters. Pint et al.⁶ found that, in an aligned SWNT film, conductivity along the direction of alignment is up to 2 orders of magnitude higher than that in the orthogonal direction. Likewise, the modulus of SWNT fibers drops 10-fold as the degree of alignment among constituent SWNTs is degraded.⁷ In terms of mismatch in electronic band structure, Fuhrer et al.⁸ showed that the junction resistance between a metallic-type and semiconducting SWNT is typically 100-fold higher than that between SWNTs with similar band structures. In SWNT macrostructures, these high-resistance junctions become bottlenecks for electron transport, leading to poor bulk conductivity. A new technique is needed to fabricate highly ordered thin films of SWNTs sorted by electronic type or enriched by chirality.

Ordered transparent conductive SWNT thin films are desirable for applications including electronic displays, touch screens, organic light-emitting devices, and photovoltaics. Recent reports show that SWNTs act as anchoring agents for liquid crystals.^{9–12} Fu et al.¹³ demonstrated a prototype liquid-crystal display (LCD) in which an aligned SWNT film serves both as the transparent conductive layer and the liquid-crystal-aligning layer, thereby eliminating one layer (e.g., polyimide)

and LCD processing steps. Ordered SWNT thin films can also template the large-scale assembly and orientational ordering of anisotropic plasmonic nanoparticles.¹⁴ Such macroscopic ordered assemblies of nanoparticles on conductive substrates are valuable for optical metamaterials and photovoltaics.^{15,16} Recent reports have shown that graphene and graphene oxide demonstrate performance and behavior similar to that of CNTs for a range of applications, including forming transparent conductive films^{17,18} and exhibiting lyotropic liquid-crystalline phases.^{19–21} Techniques developed for fabricating ordered thin films of SWNTs can be extended to graphene and graphene oxide with appropriate modifications.

In general, aligned CNT films and fibers can be fabricated by dry and wet methods. In dry methods, aligned arrays of CNTs grown by chemical vapor deposition (CVD) are “dry processed” into thin films and fibers while preserving the pre-existing alignment.^{22,23} In wet methods, orientational order is achieved by forming a nematic liquid-crystalline phase in appropriate solvents, such as superacids for pristine high-quality CNTs^{24–26} or water for CNTs that have been oxidized or stabilized by biomolecules.^{27–31} This yields well-aligned wet-spun macroscopic fibers of pristine nanotubes.^{3,24,32} Ordered films (~30 μm thick) of oxidized CNTs obtained by vacuum filtration³³ or by evaporation of solvent³⁴ have also been reported.

The current techniques for creating aligned films and fibers have limitations. Despite recent advances in CNT synthesis,³⁵

Received: January 21, 2012

Revised: June 18, 2012

Accepted: June 29, 2012

Published: June 29, 2012

growth of single-chirality SWNTs at significant scales has not yet been achieved, limiting the use of dry methods to produce single-chirality aligned SWNT films. For wet methods, the creation of a nematic phase requires high concentrations and, hence, large amounts (~ 0.1 g or more) of CNTs, which remains challenging with currently available sorting and enrichment techniques, such as density-gradient ultracentrifugation (DGU)^{36,37} and dielectrophoresis (DEP).³⁸

Herein, we present a versatile and yet simple technique for fabricating pristine SWNT thin films with high local order. The technique is based on vacuum filtration of SWNT–surfactant colloidal suspensions (Figure 1). The filtration rate is the critical parameter that controls whether the film is ordered or disordered.

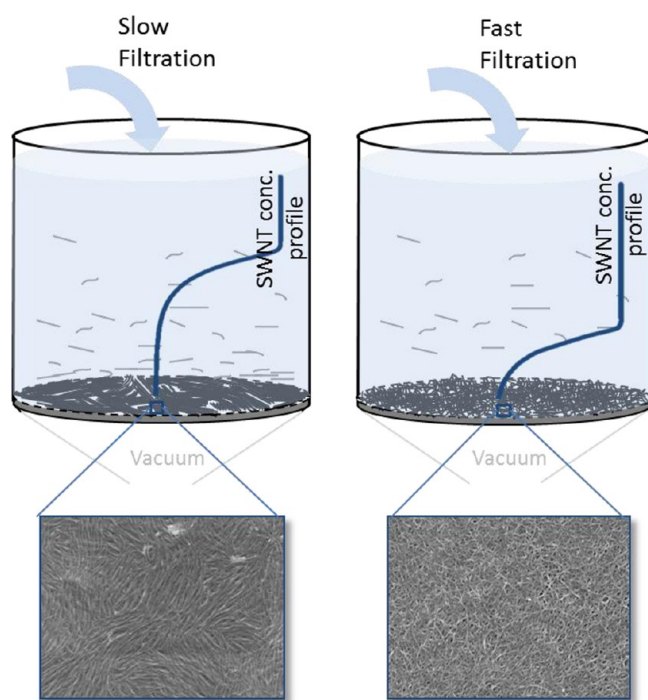


Figure 1. Schematic of the differences between slow (2 mL/h) and fast (1 mL/min) vacuum filtration. Slow filtration leads to a 30-times-thicker “high SWNT concentration region”, shown by the “SWNT conc. profile” plots (log–log scale, normalized), and a longer SWNT residence time than fast filtration. Orientational ordering of SWNTs in this region leads to the formation of nematic-like ordered thin films, as opposed to random-network films.

EXPERIMENTAL SECTION

Aqueous SWNT dispersions were prepared using surfactants and SWNTs produced by the high-pressure carbon monoxide (HiPco) process and purified at Rice University using the method outlined in O’Connell et al.³⁹ The dispersions were centrifuged for 4 h at $\sim 89000g$ on average (Sorvall Discovery 100SE Ultracentrifuge with AH-629 swing bucket rotor) to remove large SWNT bundles and undispersed material. The resultant dispersions typically consisted of 0.5–1 wt % surfactants and 30–60 ppm SWNTs as confirmed by UV–vis absorption spectroscopy (see the Supporting Information).

Vacuum filtration was performed using a laboratory vacuum line and standard microfiltration setup (Fisher Scientific) with 25-mm-diameter fritted glass filter membrane holder and polycarbonate track-etched (PCTE) filter membranes obtained

from SPI Supplies. Each SWNT film was produced by filtering 1.5–2 mL of an SWNT dispersion (30–60 mg/L concentration), keeping the filtration funnel covered with water-saturated tissue to minimize solvent evaporation. Upon completion of filtration and 30 min of drying under vacuum suction, the retentate on the filter was washed with a deionized water–ethanol mixture (50:50 v/v) to remove residual surfactant and subsequently dried in a vacuum oven for 2 h at 80 °C. The dried SWNT film on the filter membrane was immersed in a bath of *N*-methyl-2-pyrrolidone (NMP) to gently dissolve away the filter membrane, leaving behind a free-floating SWNT film that was collected on a silicon or glass substrate.

Scanning electron microscopy (SEM) of SWNT films supported on silicon substrates was carried out on a JEOL 6500F thermal field-emission electron microscope at 10–15 kV. Electro-optical property characterization was carried out on SWNT films supported on microscopy glass slides using a Zeiss Axioplan optical microscope and a Jandel microposition electrical four-point probe with a cylindrical probe head and a 1-mm probe spacing.

RESULTS AND DISCUSSION

To study the effect of the filtration rate on the film nanostructure, dispersions of SWNTs and sodium dodecylbenzene sulfonate (SDBS) were filtered through two PCTE filter membranes with different pore sizes, namely, 200 nm (filtration rate ≈ 1 mL/min) and 30 nm (filtration rate ≈ 2 mL/h).

SEM images of the resulting films (Figure 2a,b) clearly show that “fast filtration” leads to a random SWNT network, similar to that obtained in the pioneering work of Rinzler’s group,⁴⁰ whereas “slow filtration” produces local nematic ordering among SWNTs. Note that SEM imaging was performed on the top surfaces of all films. SEM of the bottom surfaces (in contact with the filter membrane) did not show conclusive evidence of ordering. Such a lack of order is likely because the deposition/adsorption of the first few SWNT layers on the filter membrane occurred in an uncontrolled manner.

The SWNTs in aqueous suspension are stabilized by micellar coating of surfactants. Given the low concentration of surfactants in suspension (slightly higher than their critical micelle concentrations), the ordering is driven by SWNTs. However, the surfactants control the interaction between SWNTs through steric and electric repulsion and can potentially affect the ordering process. To explore the role of various surfactant types on the ordering, films were fabricated from SWNT dispersions prepared using surfactants with different ionic structures: cetyltrimethylammonium bromide (CTAB, cationic) and Pluronic F87 (nonionic). The SEM images in Figure 2c,d show the similar nematic-like ordering observed in these films. The slow-filtration technique was applied to an SWNT dispersion enriched in metallic SWNTs prepared using DGU³⁷ and used in its as-produced form, containing multiple surfactants and iodixanol (the density-gradient agent). Further characterizations of the DGU SWNT dispersion are provided in the Supporting Information. Figure 3 shows the metallic-enriched SWNT dispersion and ensuing films with local nematic ordering. Interestingly, all slowly filtered films exhibited ordering, irrespective of type, quantity, and combination of surfactants used.

In addition to surfactant type and filtration rate, the concentration of SWNTs is another parameter of interest. A detailed study of multiple filtration rates and wide ranges of

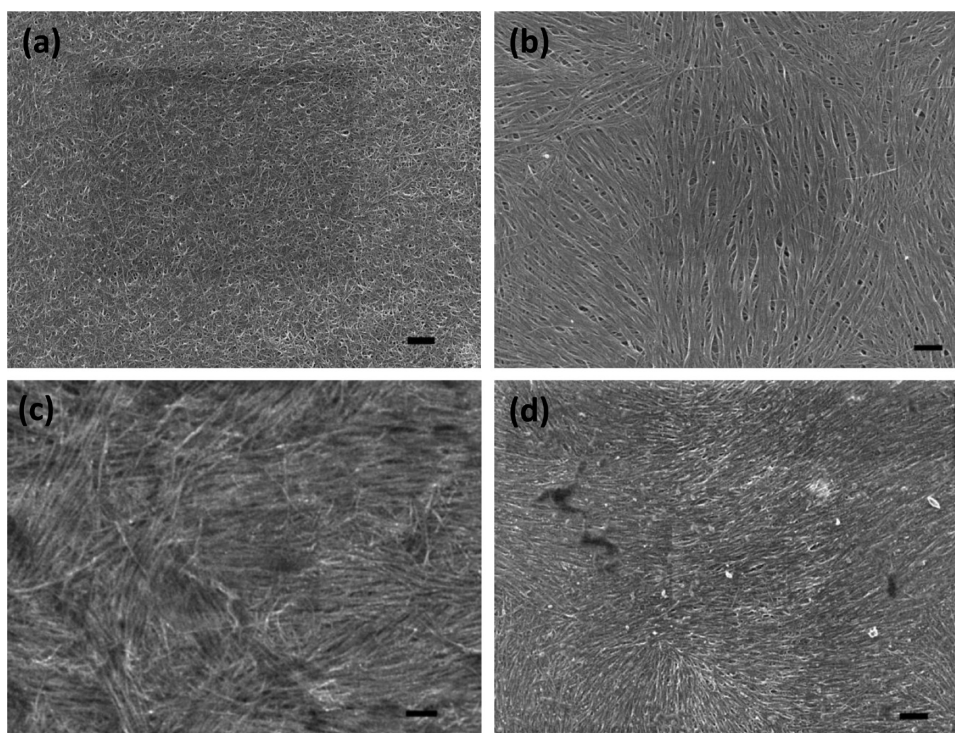


Figure 2. SEM images of SWNT thin films: (a) random SWNT network in a fast-filtration film from an SDBS dispersion, (b) nematic-like ordering in a slow-filtration film produced from same SDBS dispersion, (c,d) nematic-like ordering in slow-filtration films produced from (c) CTAB and (d) Pluronic F87 dispersions. The scale bar in each image is 200 nm.

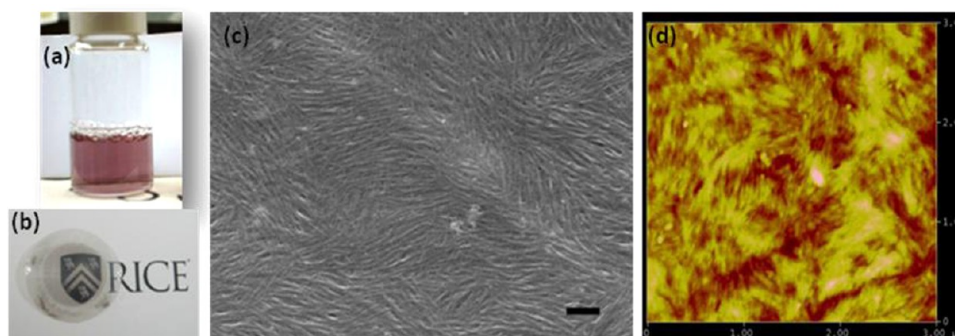


Figure 3. (a) Metallic-enriched SWNT suspension obtained from the DGU process and (b) SWNT thin film fabricated from the DGU suspension through slow filtration. (c) SEM and (d) AFM images showing the nematic-like ordering of SWNTs in the metallic-enriched film. The scale bar in c is 200 nm. The AFM image in d is $3 \mu\text{m} \times 3 \mu\text{m}$.

SWNT concentrations can potentially identify thresholds of both parameters that mark the onset of local ordering during film formation. In the case of our surfactant-stabilized SWNT dispersions, the highest achievable concentration of individualized SWNTs was limited to only 30–60 mg/L,⁴¹ so a study on the effect of variations in the SWNT concentration was not pursued in the current experiment design. The effect of CNT concentration on filtered film microstructure was studied by Shaffer et al.³³ Their studies on oxidized CNT aqueous dispersions showed that a low CNT concentration (dilute regime) was important to achieve ordering. Higher concentrations were found to lead to CNT entanglement and low rotational diffusivity, likely preventing orientational ordering during film formation and resulting in random-network films.

Further analysis of nematic ordering in SWNT films was performed using the scalar order parameter, S , which quantifies the degree of alignment among individual molecules with

respect to an average direction of orientation \mathbf{n} , known as a director. The two-dimensional scalar order parameter is defined as³³

$$S_{2D} = 2\langle \cos^2 \alpha \rangle - 1 \quad (1)$$

where α is the angle between the molecular axis and \mathbf{n} and angular brackets denote an ensemble average over the orientational distribution function (ODF). Analysis of SEM images was performed using ImageJ coupled with the OrientationJ plugin.⁴² Figure 4b depicts the microstructure of an SWNT–SDBS nematic-like film (Figure 4a), consisting of adjoining “domains” of aligned SWNTs highlighted by different false colors. The largest-fitting square cells, denoting areas of uniform SWNT alignment, were selected from these domains (Figure 4c) and analyzed to obtain an ODF for the SWNTs (Figure 4d). The angle corresponding to the intensity maximum was taken as the director ($\alpha = 0$), and the ODF

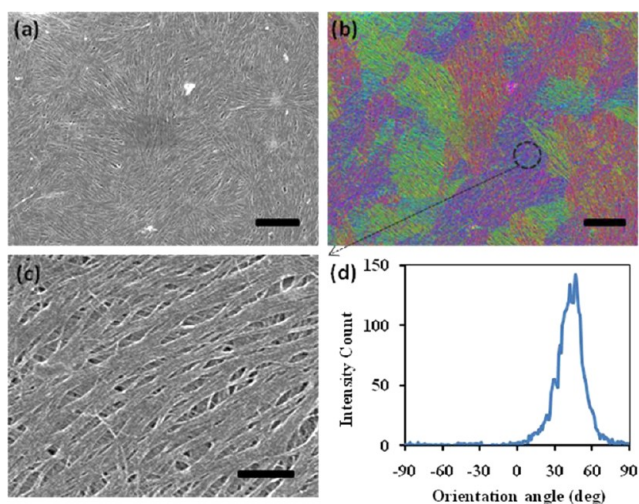


Figure 4. (a) Nematic-like ordered SWNT film from SDBS suspension (scale bar = 1 μm). (b) Domains of aligned SWNTs detected automatically by the OrientationJ plugin in ImageJ software (scale bar = 1 μm). (c) Aligned SWNTs within a single cell. (d) Orientation distribution of SWNTs in image c (scale bar 250 nm). Orientation distribution was used to calculate a two-dimensional scalar order parameter (S_{2D}) for the SWNTs. $S_{2D} \approx 0.87$ for image c.

was used to calculate an ensemble average of $\cos^2 \alpha$, which gives S_{2D} according to eq 1. As SEM cannot resolve individual SWNTs, the SWNTs were assumed to be aligned axially within each bundle, that is, $S_{2D, \text{bundle}} \approx S_{2D, \text{SWNT}}$.

S_{2D} values of numerous cells from multiple SEM images were averaged to determine an average S_{2D} value for each film, listed in Table 1 along with the average cell sizes. For the isotropic

Table 1. Average Two-Dimensional Scalar Order Parameter (S_{2D}) for a Random-Network SWNT Film from Fast Filtration and Nematic-Like Ordered SWNT Films Prepared by Slow Filtration of Different SWNT Surfactant Dispersions (Listed in the First Column), along with Average Square Cell Sizes Used for Calculation

film type	average S_{2D}	cell size (square side length, nm)
isotropic (SDBS)	0.24 ± 0.04	— ^a
CTAB	0.71 ± 0.05	797 ± 101
F87	0.76 ± 0.05	750 ± 121
SDBS	0.82 ± 0.05	1338 ± 157
metallic enriched	0.77 ± 0.09	661 ± 110

^aFor the random-network film, a series of square cells with sides ranging from 200 to 2500 nm was used.

film, the average S_{2D} value was calculated from a series of cell sizes ranging from 200 to 2500 nm; hence, no particular cell size is reported. The significantly higher S_{2D} of slow-filtration nematic-like films can be readily observed. The average cell (domain) size in the ordered films varied with the type of surfactant used in the initial dispersion. This is likely due to the fact that surfactants differ in their effectiveness in dispersing SWNTs; the fraction of SWNTs dispersed as individuals versus bundles and the average length and diameter of SWNT bundles are functions of the surfactant used. These differences could result in different domain sizes in the ordered films. Other factors possibly affecting the domain sizes and potential ways to fabricate larger domains are discussed later in this article.

SWNT thin films were also characterized for electro-optical properties. Under cross-polarized light microscopy, the films did not show any distinguishable birefringence, probably due to the small size of the domains compared to the optical resolution. The optical transmission (65–70% transparent at 550 nm) indicated the film thickness to be in the range of 100–200 nm. The electrical resistance of the films was measured in the form of “sheet resistance” using a four-point probe, which is a commonly employed technique for thin films.^{40,43} Both locally ordered and disordered films showed similar properties (300–350 Ω/sq for 65–70% transmission at 550-nm wavelength, for unsorted and metallic-enriched films). This is likely due to the fact that the measurement length scale (probe spacing ≈ 1 mm) was much larger than the size of the ordered domains (hundreds of nanometers). Thus, the values obtained under these conditions are indicative of the “average” resistance of the entire film (2 cm in diameter) and insensitive to any ordering present at a much smaller scale.

The local nematic-like ordering of SWNTs is clearly caused by the slow filtration process. As the solvent is removed by filtration, a concentration gradient develops in the filtration funnel; SWNTs increasingly concentrate near the filter membrane. Once the SWNT concentration in this high-concentration region exceeds the isotropic–nematic transition point, SWNTs begin to align spontaneously. The low filtration rate affects this process in two ways: First, it yields a less steep concentration gradient and hence a thicker high-concentration region; the characteristic thickness of this region is $\delta_{\text{conc}} \propto D/v_f$, where D is the translational diffusivity of the SWNTs and v_f is the average fluid velocity (which is a function of filtration speed). Second, SWNTs move more slowly and therefore have sufficient time to reorient into locally ordered domains while traversing the high-concentration region before depositing on the filter membrane.

We estimated the SWNT concentration profile in the liquid dispersion inside the filtration funnel during the filtration process. The steady-state equation of continuity can be expressed as $v_f \cdot \nabla c = -D \nabla^2 c$, where c is the SWNT mass fraction and is a function of distance from the filter (z). The fluid velocity, v_f , was calculated from the filtration rate (slow filtration, 2 mL/h; fast filtration, 1 mL/min) and the filtration-membrane/SWNT-film diameter (2 cm). Assuming uniform flow across the filtration membrane, this equation was solved in one dimension to obtain the SWNT concentration profile $c(z) = (C_0 - C_b)e^{-v_f z/D} + C_b$ (where C_b represents the SWNT concentration in the bulk fluid). The SWNT concentration at the surface of filter membrane (or developing wet film) was set to 20 vol% ($C_0 = 0.2$). The packing density of dry SWNT films has been observed to be around 30–50%.^{44,45} The density of wet-cast films is expected to be slightly lower. The SWNT concentration in the bulk fluid was $C_b = 4 \times 10^{-5}$ (40 ppm), as measured by UV–vis absorption spectroscopy of the initial dispersion (details are provided in the Supporting Information). The validity of the simulated parameters was confirmed by monitoring the total SWNT mass in the system, that is, the total SWNT mass initially poured into the filtration funnel versus the SWNT mass at a steady state during filtration calculated from simulation. SWNT concentration profiles for fast and slow filtration are depicted in Figure 1, shown on a log–log scale to highlight the high-concentration region. The high-concentration region for slow filtration was typically ~ 30 times thicker than that for fast filtration.

The time required for SWNTs to travel from a region with $c \approx c_{\text{biphasic}}$ (i.e., z_{biphasic}), where c_{biphasic} is the concentration marking the onset of the biphasic region for a lyotropic system and z_{biphasic} is the corresponding distance from the filter, to the filter membrane ($z = 0$) can be defined as the residence time (t_{res}) of SWNTs in the high-concentration region; it was calculated using the expression $t_{\text{res}} = \int_{z_{\text{biphasic}}}^{z=0} v_{\text{SWNT}}^{-1} dz$. For HiPco SWNTs, assuming noninteracting rods, $c_{\text{biphasic}} \approx 4000$ ppm;^{25,28,46} attractive interactions would lower this threshold. z_{biphasic} was calculated from the SWNT concentration profile, and the SWNT velocity was evaluated using the expression $v_{\text{SWNT}} = v_f - D(\nabla c/c)$. For slow filtration $t_{\text{res}} \sim 1$ s, whereas for fast filtration, $t_{\text{res}} \sim 1$ ms. In dilute SWNT dispersions, SWNTs have a rotational diffusivity of $D_R \approx 250$ s⁻¹,⁴⁷ giving a characteristic time scale (of Brownian rotation) of $\tau \sim 1$ ms. Intuitively, residence times shorter than this characteristic time make reorientation and alignment of SWNTs before they become immobilized into a film very unlikely.

Previous studies^{48,49} (on thermotropic liquid crystals) have shown that isotropic-to-nematic phase transitions typically involve three stages: (1) nucleation, comprising independent nucleation of multiple ordered domains, with no correlation between directors of different domains; (b) domain growth, comprising a period of domain size growth, typically following the dynamical scaling law $r_d \sim t^{0.5}$, where r_d is the domain diameter and t is the time; and (c) healing, comprising healing of domain boundaries and dynamics of liquid-crystal defects. The staggered domain structure of nematic-like SWNT films suggests that SWNT ordering during slow filtration likely follows a similar developmental pathway but lacks a “healing stage”, likely due to consolidation of SWNTs into a solid (or gel-like) film. This explains the relatively small domain sizes observed in the films. SWNT films with larger domain sizes can potentially be obtained by increasing the residence time (t_{res}). Possible ways of achieving longer residence times include further reducing the filtration rate and varying the SWNT length. Further insights can be drawn from the work of Song and Windle⁵⁰ on liquid-crystalline thin films of multiwalled carbon nanotubes (MWNTs), where they observed a strong dependence of domain size on both the stiffness (diameter) and the length of the constituent MWNTs.

CONCLUSIONS

We have presented a simple modification to the vacuum filtration technique for fabricating SWNT thin films with local nematic-like ordering. This technique is applicable to a number of aqueous SWNT suspensions, irrespective of type, quantity, and combination of surfactants present, as well as metallic-enriched SWNT dispersions as-produced by DGU. Scalar order parameter calculations show a high degree of local ordering among SWNTs in the film. The local ordering among SWNTs however, did not affect the large-scale sheet resistance measured on the entire film. Further engineering can potentially lead to fabrication of domains of larger dimensions and isolation of such domains with uniform alignment. Such ordered films of pristine SWNTs and the isolated domains of uniform alignment can serve as useful functional materials and a platform for patterned deposition of nanoparticles and development of metamaterials, electrodes, and transparent conductive coatings.

ASSOCIATED CONTENT

Supporting Information

Additional details on the preparation and characterization of regular SWNT dispersions and metallic-enriched dispersions. This material is available free of charge via the Internet at <http://pubs.acs.org>.

AUTHOR INFORMATION

Corresponding Author

*E-mail: mp@rice.edu.

Present Address

[†]Institute of Materials Science, University of Connecticut, 97 North Eagleville Road, Unit 3136, Storrs, CT 06269-3136, USA.

Notes

The authors declare no competing financial interest.

ACKNOWLEDGMENTS

We thank Ivan Smalyukh, Alex Lee, Jaewook Nam, and Natnael Behabtu for valuable input. Funding was provided by Air Force Research Laboratory Grant FA 8650-07-2-5061 (managed by CONTACT), Air Force Office of Scientific Research Grant FA9550-09-1-0590, Welch Foundation Grant C-1668, a J. Evans-Attwell postdoctoral fellowship, and U.S. Army Corps of Engineers Environmental Quality and Installation Program Grant W912HZ-08-C-0054.

REFERENCES

- (1) Odom, T. W.; Huang, J. L.; Kim, P.; Lieber, C. M. Atomic Structure and Electronic Properties of Single-Walled Carbon Nanotubes. *Nature* **1998**, *391*, 62.
- (2) Tans, S. J.; Devoret, M. H.; Dai, H. J.; Thess, A.; Smalley, R. E.; Geerligs, L. J.; Dekker, C. Individual Single-Wall Carbon Nanotubes as Quantum Wires. *Nature* **1997**, *386*, 474.
- (3) Behabtu, N.; Green, M. J.; Pasquali, M. Carbon Nanotube-Based Neat Fibers. *Nano Today* **2008**, *3*, 24.
- (4) Dan, B.; Irvin, G. C.; Pasquali, M. Continuous and Scalable Fabrication of Transparent Conducting Carbon Nanotube Films. *ACS Nano* **2009**, *3*, 835.
- (5) Bachilo, S. M.; Strano, M. S.; Kittrell, C.; Hauge, R. H.; Smalley, R. E.; Weisman, R. B. Structure-Assigned Optical Spectra of Single-Walled Carbon Nanotubes. *Science* **2002**, *298*, 2361.
- (6) Pint, C. L.; Xu, Y. Q.; Morosan, E.; Hauge, R. H. Alignment Dependence of One-Dimensional Electronic Hopping Transport Observed in Films of Highly Aligned, Ultralong Single-Walled Carbon Nanotubes. *Appl. Phys. Lett.* **2009**, *94*, 182107.
- (7) Liu, T.; Kumar, S. Effect of Orientation on the Modulus of SWNT Films and Fibers. *Nano Lett.* **2003**, *3*, 647.
- (8) Fuhrer, M. S.; Nygard, J.; Shih, L.; Forero, M.; Yoon, Y. G.; Mazzone, M. S. C.; Choi, H. J.; Ihm, J.; Louie, S. G.; Zettl, A.; McEuen, P. L. Crossed Nanotube Junctions. *Science* **2000**, *288*, 494.
- (9) Russell, J. M.; Oh, S. J.; LaRue, I.; Zhou, O.; Samulski, E. T. Alignment of Nematic Liquid Crystals Using Carbon Nanotube Films. *Thin Solid Films* **2006**, *509*, 53.
- (10) Park, K. A.; Lee, S. M.; Lee, S. H.; Lee, Y. H. Anchoring a Liquid Crystal Molecule on a Single-Walled Carbon Nanotube. *J. Phys. Chem. C* **2007**, *111*, 1620.
- (11) Basu, R.; Iannacchione, G. S. Nematic Anchoring on Carbon Nanotubes. *Appl. Phys. Lett.* **2009**, *95*, 173113.
- (12) van der Schoot, P.; Popa-Nita, V.; Kralj, S. Alignment of Carbon Nanotubes in Nematic Liquid Crystals. *J. Phys. Chem. B* **2008**, *112*, 4512.
- (13) Fu, W. Q.; Liu, L.; Jiang, K. L.; Li, Q. Q.; Fan, S. S. Super-Aligned Carbon Nanotube Films as Aligning Layers and Transparent Electrodes for Liquid Crystal Displays. *Carbon* **2010**, *48*, 1876.

- (14) Dan, B.; Wingfield, T.; Evans, J. S.; Mirri, F.; Pint, C.; Pasquali, M.; Smalyukh, I. I. Templating of Self-Alignment Patterns of Anisotropic Gold Nanoparticles on Ordered Swnt Macrostructures. *ACS Appl. Mater. Interfaces* **2011**, *3*, 3718.
- (15) Shalaev, V. M. Optical Negative-Index Metamaterials. *Nat. Photonics* **2007**, *1*, 41.
- (16) Atwater, H. A.; Polman, A. Plasmonics for Improved Photovoltaic Devices. *Nat. Mater.* **2010**, *9*, 205.
- (17) Bae, S.; Kim, H.; Lee, Y.; Xu, X.; Park, J. S.; Zheng, Y.; Balakrishnan, J.; Lei, T.; Kim, H. R.; Song, Y. I. Roll-to-Roll Production of 30-Inch Graphene Films for Transparent Electrodes. *Nat. Nanotechnol.* **2010**, *5*, 574.
- (18) Wang, X.; Zhi, L.; Müllen, K. Transparent, Conductive Graphene Electrodes for Dye-Sensitized Solar Cells. *Nano Lett.* **2008**, *8*, 323.
- (19) Behabtu, N.; Lomeda, J. R.; Green, M. J.; Higginbotham, A. L.; Sinitiskii, A.; Kosynkin, D. V.; Tsentelovich, D.; Parra-Vasquez, A. N. G.; Schmidt, J.; Kesselman, E. Spontaneous High-Concentration Dispersions and Liquid Crystals of Graphene. *Nat. Nanotechnol.* **2010**, *5*, 406.
- (20) Dan, B.; Behabtu, N.; Martinez, A.; Evans, J. S.; Kosynkin, D. V.; Tour, J. M.; Pasquali, M.; Smalyukh, I. I. Liquid Crystals of Aqueous, Giant Graphene Oxide Flakes. *Soft Matter* **2011**, *7*, 11154.
- (21) Kim, J. E.; Han, T. H.; Lee, S. H.; Kim, J. Y.; Ahn, C. W.; Yun, J. M.; Kim, S. O. Graphene Oxide Liquid Crystals. *Angew. Chem., Int. Ed.* **2011**, *50*, 3043.
- (22) Pint, C. L.; Xu, Y. Q.; Moghazy, S.; Cherukuri, T.; Alvarez, N. T.; Haroz, E. H.; Mahzooni, S.; Doorn, S. K.; Kono, J.; Pasquali, M.; Hauge, R. H. Dry Contact Transfer Printing of Aligned Carbon Nanotube Patterns and Characterization of Their Optical Properties for Diameter Distribution and Alignment. *ACS Nano* **2010**, *4*, 1131.
- (23) Zhang, M.; Fang, S. L.; Zakhidov, A. A.; Lee, S. B.; Aliev, A. E.; Williams, C. D.; Atkinson, K. R.; Baughman, R. H. Strong, Transparent, Multifunctional, Carbon Nanotube Sheets. *Science* **2005**, *309*, 1215.
- (24) Davis, V. A.; Parra-Vasquez, A. N. G.; Green, M. J.; Rai, P. K.; Behabtu, N.; Prieto, V.; Booker, R. D.; Schmidt, J.; Kesselman, E.; Zhou, W.; Fan, H.; Adams, W. W.; Hauge, R. H.; Fischer, J. E.; Cohen, Y.; Talmon, Y.; Smalley, R. E.; Pasquali, M. True Solutions of Single-Walled Carbon Nanotubes for Assembly into Macroscopic Materials. *Nat. Nanotechnol.* **2009**, *4*, 830.
- (25) Green, M. J.; Parra-Vasquez, A. N. G.; Behabtu, N.; Pasquali, M. Modeling the Phase Behavior of Polydisperse Rigid Rods with Attractive Interactions with Applications to Single-Walled Carbon Nanotubes in Superacids. *J. Chem. Phys.* **2009**, *131*, 084901.
- (26) Rai, P. K.; Pinnick, R. A.; Parra-Vasquez, A. N. G.; Davis, V. A.; Schmidt, H. K.; Hauge, R. H.; Smalley, R. E.; Pasquali, M. Isotropic–Nematic Phase Transition of Single-Walled Carbon Nanotubes in Strong Acids. *J. Am. Chem. Soc.* **2006**, *128*, 591.
- (27) Song, W. H.; Kinloch, I. A.; Windle, A. H. Nematic Liquid Crystallinity of Multiwall Carbon Nanotubes. *Science* **2003**, *302*, 1363.
- (28) Moulton, S. E.; Maugey, M.; Poulin, P.; Wallace, G. G. Liquid Crystal Behavior of Single-Walled Carbon Nanotubes Dispersed in Biological Hyaluronic Acid Solutions. *J. Am. Chem. Soc.* **2007**, *129*, 9452.
- (29) Badaire, S.; Zakri, C.; Maugey, M.; Derre, A.; Barisci, J. N.; Wallace, G.; Poulin, P. Liquid Crystals of DNA-Stabilized Carbon Nanotubes. *Adv. Mater.* **2005**, *17*, 1673.
- (30) Puech, N.; Grelet, E.; Poulin, P.; Blanc, C.; van der Schoot, P. Nematic Droplets in Aqueous Dispersions of Carbon Nanotubes. *Phys. Rev. E* **2010**, *82*, 020702.
- (31) Ao, G.; Nepal, D.; Aono, M.; Davis, V. A. Cholesteric and Nematic Liquid Crystalline Phase Behavior of Double-Stranded DNA Stabilized Single-Walled Carbon Nanotube Dispersions. *ACS Nano* **2011**, *5*, 1450.
- (32) Ericson, L. M.; Fan, H.; Peng, H. Q.; Davis, V. A.; Zhou, W.; Sulpizio, J.; Wang, Y. H.; Booker, R.; Vavro, J.; Guthy, C.; Parra-Vasquez, A. N. G.; Kim, M. J.; Ramesh, S.; Saini, R. K.; Kittrell, C.; Lavin, G.; Schmidt, H.; Adams, W. W.; Billups, W. E.; Pasquali, M.; Hwang, W. F.; Hauge, R. H.; Fischer, J. E.; Smalley, R. E. Macroscopic, Neat, Single-Walled Carbon Nanotube Fibers. *Science* **2004**, *305*, 1447.
- (33) Shaffer, M. S. P.; Fan, X.; Windle, A. H. Dispersion and Packing of Carbon Nanotubes. *Carbon* **1998**, *36*, 1603.
- (34) Shimoda, H.; Oh, S. J.; Geng, H. Z.; Walker, R. J.; Zhang, X. B.; McNeil, L. E.; Zhou, O. Self-Assembly of Carbon Nanotubes. *Adv. Mater.* **2002**, *14*, 899.
- (35) Harutyunyan, A. R.; Chen, G. G.; Paronyan, T. M.; Pigos, E. M.; Kuznetsov, O. A.; Hewaparakrama, K.; Kim, S. M.; Zakharov, D.; Stach, E. A.; Sumanasekera, G. U. Preferential Growth of Single-Walled Carbon Nanotubes with Metallic Conductivity. *Science* **2009**, *326*, 116.
- (36) Arnold, M. S.; Green, A. A.; Hulvat, J. F.; Stupp, S. I.; Hersam, M. C. Sorting Carbon Nanotubes by Electronic Structure Using Density Differentiation. *Nat. Nanotechnol.* **2006**, *1*, 60.
- (37) Haroz, E. H.; Rice, W. D.; Lu, B. Y.; Ghosh, S.; Hauge, R. H.; Weisman, R. B.; Doorn, S. K.; Kono, J. Enrichment of Armchair Carbon Nanotubes Via Density Gradient Ultracentrifugation: Raman Spectroscopy Evidence. *ACS Nano* **2010**, *4*, 1955.
- (38) Krupke, R.; Hennrich, F.; von Lohneysen, H.; Kappes, M. M. Separation of Metallic from Semiconducting Single-Walled Carbon Nanotubes. *Science* **2003**, *301*, 344.
- (39) O'Connell, M. J.; Boul, P.; Ericson, L. M.; Huffman, C.; Wang, Y. H.; Haroz, E.; Kuper, C.; Tour, J.; Ausman, K. D.; Smalley, R. E. Reversible Water-Solubilization of Single-Walled Carbon Nanotubes by Polymer Wrapping. *Chem. Phys. Lett.* **2001**, *342*, 265.
- (40) Wu, Z. C.; Chen, Z. H.; Du, X.; Logan, J. M.; Sippel, J.; Nikolou, M.; Kamaras, K.; Reynolds, J. R.; Tanner, D. B.; Hebard, A. F.; Rinzler, A. G. Transparent, Conductive Carbon Nanotube Films. *Science* **2004**, *305*, 1273.
- (41) Duque, J. G.; Parra-Vasquez, A. N. G.; Behabtu, N.; Green, M. J.; Higginbotham, A. L.; Price, B. K.; Leonard, A. D.; Schmidt, H. K.; Lounis, B.; Tour, J. M.; Doorn, S. K.; Cognet, L.; Pasquali, M. Diameter-Dependent Solubility of Single-Walled Carbon Nanotubes. *ACS Nano* **2010**, *4*, 3063.
- (42) Fonck, E.; Feigl, G. G.; Fasel, J.; Sage, D.; Unser, M.; Rufenacht, D. A.; Stergiopoulos, N. Effect of Aging on Elastin Functionality in Human Cerebral Arteries. *Stroke* **2009**, *40*, 2552.
- (43) Gruner, G. Carbon Nanotube Films for Transparent and Plastic Electronics. *J. Mater. Chem.* **2006**, *16*, 3533.
- (44) Jeon, T. I.; Kim, K. J.; Kang, C.; Maeng, I. H.; Son, J. H.; An, K. H.; Lee, J. Y.; Lee, Y. H. Optical and Electrical Properties of Preferentially Anisotropic Single-Walled Carbon-Nanotube Films in Terahertz Region. *J. Appl. Phys.* **2004**, *95*, 5736.
- (45) Lyons, P. E.; De, S.; Blighe, F.; Nicolosi, V.; Pereira, L. F. C.; Ferreira, M. S.; Coleman, J. N. The Relationship between Network Morphology and Conductivity in Nanotube Films. *J. Appl. Phys.* **2008**, *104*, 044302.
- (46) Wensink, H. H.; Vroege, G. J. Isotropic–Nematic Phase Behavior of Length-Polydisperse Hard Rods. *J. Chem. Phys.* **2003**, *119*, 6868.
- (47) Duggal, R.; Pasquali, M. Dynamics of Individual Single-Walled Carbon Nanotubes in Water by Real-Time Visualization. *Phys. Rev. Lett.* **2006**, *96*, 246104.
- (48) Bradac, Z.; Kralj, S.; Zumer, S. Molecular Dynamics Study of the Isotropic–Nematic Quench. *Phys. Rev. E* **2002**, *65*, 021705.
- (49) Chen, X. M.; Hamlington, B. D.; Shen, A. Q. Isotropic-to-Nematic Phase Transition in a Liquid-Crystal Droplet. *Langmuir* **2008**, *24*, 541.
- (50) Song, W.; Windle, A. H. Size-Dependence and Elasticity of Liquid-Crystalline Multiwalled Carbon Nanotubes. *Adv. Mater.* **2008**, *20*, 3149.